Title
Heterogeneous oxidation of a phosphocholine on synthetic sea salt by ozone at room temperature

Journal
Physical Chemistry Chemical Physics, 15(6)

ISSN
1463-9076 1463-9084

Authors
Dilbeck, Christopher W
Finlayson-Pitts, Barbara J

Publication Date
2013

DOI
10.1039/c2cp43665e

Peer reviewed

PCCP

RSC Publishing

PAPER

View Article Online
View Journal | View Issue

Cite this: *Phys. Chem. Chem. Phys.*, 2013, **15**, 1990

Heterogeneous oxidation of a phosphocholine on synthetic sea salt by ozone at room temperature

Christopher W. Dilbeck and Barbara J. Finlayson-Pitts*

Received 16th October 2012,
Accepted 6th December 2012

DOI: 10.1039/c2cp43665e

www.rsc.org/pccp

The ozonolysis of 1-palmitoyl-2-oleoyl-*sn-glycero*-3-phosphocholine (POPC) adsorbed on salt mixtures as models for sea-salt particles was studied in real time using diffuse reflection infrared Fourier transform spectrometry (DRIFTS) at room temperature with and without added water vapor. The salt substrates were a mixture of $MgCl_2 \cdot 6H_2O$ with NaCl or a commercially available synthetic sea salt. Ozone concentrations ranged from (0.25 to 3.9) $\times$ 10^{13} molecules cm^{-3} (0.1–1.6 ppm). The major products identified by FTIR and confirmed using matrix-assisted laser desorption/ionization (MALDI) mass spectrometry were the secondary ozonide (SOZ) and a phospholipid aldehyde and carboxylic acid formed by scission of the double bond. The reaction probabilities for the two substrates were similar, $\gamma = (6\text{–}7) \times 10^{-7}$, with an estimated overall uncertainty of a factor of two. The presence of water vapor decreased the yield of SOZ relative to the products formed by C=C scission, but also increased the availability of the double bond for reaction, particularly on the less hygroscopic commercial sea-salt substrate. Thus, water not only affects the mechanisms and products, but also the structure of the phospholipid on the salt in a manner that affects its reactivity. The results of these studies suggest that the reactivity and products of oxidation of unsaturated phospholipids on sea-salt particles in air will be very sensitive to the nature and phase of the substrate, the amount of water present, and whether there is phase separation between the organics and the inorganic salt mixture.

Introduction

Sea-salt aerosol (SSA) plays an important role in many chemical and physical atmospheric processes, with an estimated annual production of 5×10^{15} g.[1] It is a large contributor to atmospheric particulate matter, especially over oceans.[1–7] Aerosol particles adversely affect visibility and human health, and also have well-documented effects on the chemistry[8,9] and radiative balance of the atmosphere.[6] Thus, they affect incoming and outgoing radiation directly by scattering light, and indirectly through their ability to act as cloud condensation nuclei and their effects on cloud albedo.[6] This is a major area of uncertainty in attributing sources of climate change.[6]

SSA particles are formed predominantly *via* bubble bursting on the surface of the ocean[1–4] and acquire an organic coating during this process.[10–13] Organic compounds in SSA particles are expected to come from organisms and their decomposition in the ocean, among other sources, and include lipids, proteins, and carbohydrates.[14–21] The organic component of SSA can make up more than half of SSA particles by mass during phytoplankton blooms.[22,23] The presence of organics will affect the particles' properties and ability to act as cloud condensation nuclei,[24–26] as well as the exchange of gases with the atmosphere.[9] Understanding the oxidation of the organic component of SSA particles in the atmosphere is important because this may modify the particle properties.[27]

In previous studies,[28] the ozonolysis of 1-oleoyl-2-palmitoyl-*sn-glycero*-3-phosphocholine (OPPC) on NaCl was studied using diffuse reflection infrared Fourier transform spectrometry (DRIFTS).[29–32] This technique, which can be used with any infrared transparent substrate,[31,33] allows changes in the solid mixture to be followed as a function of reaction time. While NaCl is the major component of sea salt, it may not represent all of the properties found in sea-salt particles, which are much more complex mixtures.[1,34,35] A significant difference is the presence of hygroscopic salts such as magnesium chloride. Magnesium is the second most abundant cation in sea salt. The molar ratio of sodium to magnesium in sea salt is 8.9:1.[34,35]

In this work, the room temperature ozone oxidation of the phospholipid 1-palmitoyl-2-oleoyl-*sn-glycero*-3-phosphocholine (POPC), a naturally-occurring isomer of OPPC (which is expected to have the same reactivity as OPPC), adsorbed on

Department of Chemistry, University of California Irvine, Irvine, CA 92697-2025, USA. E-mail: bjfinlay@uci.edu; Fax: +1 949 824-2420; Tel: +1 949 824-7670

either a mixture of $MgCl_2 \cdot 6H_2O$ with NaCl or on a commercially available synthetic aquarium sea salt was studied. It is shown that even small amounts of adsorbed water have an effect on the product distributions, as well as on the availability of the double bond for reaction and hence the reaction probability. Under atmospheric conditions, these model systems may be applicable to mixed sea-salt/organic particles where there is liquid–liquid phase separation.[36–39]

Experimental section

Sample preparation

Synthetic sea salt (Instant Ocean®, Spectrum Brands) was used as a model for sea-salt particles. Its elemental composition is similar to that given for synthetic sea salt by Langer *et al.*,[40] in terms of the major ions. The salt was ground using a Wig-L-Bug® (Crescent Dental Mfg.) for 5 minutes to generate particles in the size range of 1–10 μm,[32,41] optimum for DRIFTS analysis.[31] Finely-ground Instant Ocean® (IO) powder (0.50 g) was mixed with 0.40 mL of a solution of POPC in a hexane–ethanol mixture (25 mg of POPC in 9 mL hexane and 1 mL ethanol). An area per molecule of 6×10^{-15} cm^2 was assumed based on previous studies of the surface pressure–area isotherms of OPPC films on water.[42,43] This area per molecule corresponds to a surface concentration of 1.6×10^{14} molecules cm^{-2}. The relative amounts of POPC and salt were chosen so that the phospholipid would form a monolayer if evenly distributed over cubic salt particles 2 μm on a side. The mixture of POPC and Instant Ocean® was stirred under a stream of ultra-high purity (UHP) N_2 (Oxygen Service Company, 99.9995%) to evaporate the solvent. The coated salt, referred to as POPC/IO, was ground for a few seconds in a mortar and pestle to break up clumps and placed in a glass trap that was evacuated to a pressure of $\sim 10^{-3}$ Torr for one hour on a vacuum manifold to remove weakly bound water. A separate set of samples was also prepared by mixing $MgCl_2 \cdot 6H_2O$ (0.14 g) with NaCl (0.36 g) and POPC solution (0.40 mL) to yield samples with a molar ratio of sodium to magnesium of 8.9 : 1.[34,35] The POPC/$MgCl_2 \cdot 6H_2O$/NaCl samples were treated as described above for POPC/IO samples.

DRIFTS

Reactions of POPC/IO or POPC/$MgCl_2 \cdot 6H_2O$/NaCl with ozone were performed at 293–295 K at a pressure of 1 atm in a gas flow system described in detail elsewhere.[28] Changes in the adsorbed organic were monitored as a function of time using DRIFTS. The DRIFTS sample holder was filled with 0.35 g of POPC/IO or POPC/$MgCl_2 \cdot 6H_2O$/NaCl by packing it into the sample cup with a press[44] using manual pressure. A flow of either dry or humidified UHP N_2 was pumped through the sample overnight to stabilize it with respect to adsorbed water. Extensive drying or heating of the $MgCl_2 \cdot 6H_2O$ and IO was avoided in order to minimize removal of waters of hydration and formation of Mg(OH)Cl and/or MgO, which are less soluble and hygroscopic.[45,46] The solubilities of Mg(OH)Cl and MgO in methanol are 1.26×10^{-3} g per 100 mL and 1.46×10^{-4} g per 100 mL, respectively.[47] To test for formation of Mg(OH)Cl and/or MgO, 500 mg of the $MgCl_2 \cdot 6H_2O$/NaCl mixture was treated as described above for the POPC coated samples before an experiment, *i.e.*, it was dried under vacuum for one hour, placed in the DRIFTS sample holder and N_2 was pumped through the sample overnight. When this sample was dissolved in 50 mL of methanol, no insoluble material was observed visually. In contrast, 1 mg of MgO (EMD, 95%) was clearly visible when mixed in 50 mL methanol. Therefore, if dehydration forms MgO, less than 4% by moles of the $MgCl_2 \cdot 6H_2O$ is converted to MgO during sample preparation. If the product of dehydration was Mg(OH)Cl, and assuming 1 mg of Mg(OH)Cl precipitate beyond the solubility limit would also be evident in 50 mL methanol, then an upper limit of 3% of the $MgCl_2 \cdot 6H_2O$ was converted to Mg(OH)Cl by this process.

To humidify the N_2, it was passed through a water-filled bubbler (Millipore Milli-Q, 18.2 MΩ cm) and then into a 5 L mixing bulb where it was diluted with dry N_2 to obtain the desired water concentration. The relative humidity (RH) and temperature were measured in the mixing bulb using a Vaisala HMP238 sensor. Studies could only be carried out up to 1.4×10^{17} molecules H_2O cm^{-3} (20% RH) because of large and irreproducible changes in the baseline at higher water vapor concentrations, and very strong absorption of infrared radiation by water in large regions of the spectrum. In addition, the deliquescence point[48] of $MgCl_2 \cdot 6H_2O$ is 33% RH, so that staying well below this is important to maintain the integrity of the solid salt.

Ozone was generated by flowing a mixture of UHP oxygen gas (99.993%, Oxygen Service Co.) and UHP helium gas (99.9995%, Oxygen Service Co.) through a housing containing a mercury pen-ray lamp (Jelight Co. Inc., Double Bore 78-2046). Ozone was diluted with air (Ultrapure Air, Scott-Marrin, total hydrocarbons as $CH_4 < 0.01$ ppm; $CO < 0.01$ ppm; $NO_x < 0.001$ ppm; $SO_2 < 0.001$ ppm) to produce concentrations of $(0.25 \text{ to } 3.9) \times 10^{13}$ O_3 cm^{-3} (0.1–1.6 ppm) as measured with a Teledyne Advanced Pollution Instrumentation Model 400 Ozone Analyzer. The instrument was calibrated with an Ocean Optics HR4000CG UV–VIS–NIR spectrometer using the measured absorption at 254 nm as ozone flowed through a 30 cm cell, and the known absorption cross-section ($\sigma = 5.0 \times 10^{-18}$ cm^2 $molecule^{-1}$, base 10)[49] of ozone at 254 nm. Experiments were conducted (1) without added water vapor and with ozone concentrations of 0.25, 1.25, 2.5 and 3.9×10^{13} molecules cm^{-3}; and (2) at 3.9×10^{13} O_3 cm^{-3} with 0.34, 0.68, and 1.4×10^{17} molecules cm^{-3} added water vapor (5, 10, and 20% RH, respectively).

MALDI-TOF-MS

Matrix-assisted laser-desorption/ionization-time-of-flight-mass spectrometry (MALDI-TOF-MS) was used to confirm the identification of products after reaction with ozone. Samples were prepared for mass spectrometric analysis by dissolving 20 mg of the reacted sample in a mixture of 80 μL water (Fisher, HPLC grade) with 80 μL acetonitrile (OmniSolv, HPLC grade), mixing on a vortex mixer, and micro-centrifuging for 30 seconds. A 0.5 μL

sample of this solution was placed on a 384-well stainless steel plate and 0.5 μL of a saturated solution of 2,5-dihydroxybenzoic acid (Fluka, 99.5%) in 2:1 water : acetonitrile was added as the matrix material. Positive ion mass spectra were recorded using 1000–5000 accumulated shots with the laser pulsing at 400 Hz in reflectron mode on an AB/Sciex 5800 TOF/TOF instrument.

Results and discussion

Identification of products and branching ratios

DRIFTS spectra of POPC/NaCl, POPC/IO and IO alone are shown in Fig. 1 (POPC structure is shown in Fig. 1a). Spectra are given as $\log_{10}(S_0/S_1)$ where S_0 is the single beam spectrum of NaCl and S_1 is the single beam spectrum of the sample. This approach was established in earlier studies of similar systems[32] to be more appropriate for quantitative analysis than the Kubelka–Munk function. Because NaCl is infrared transparent, the peaks in Fig. 1a can be assigned to functional groups in the phospholipid. Peaks due to the hydrocarbon groups occur at 2960 cm^{-1} ($\nu_{asym\ str}$, $-CH_3$), 2920 cm^{-1} ($\nu_{asym\ str}$, $-CH_2-$) and 2850 cm^{-1} ($\nu_{sym\ str}$, $-CH_2-$), and 1470 cm^{-1} ($\nu_{scissor}$, $-CH_2-$, $\nu_{asym\ def}$, $-N(CH_3)_3^+$).[50] A smaller peak due to the vinyl H–C=C stretch at 3008 cm^{-1} is also seen. Contributions from the PO_2^- group at 1255 and 1095 cm^{-1}, the two ester carbonyl groups stretch at 1735 cm^{-1} and the C(O)–O–C asymmetric stretch at 1180 cm^{-1} are also evident (the symmetric stretch of the latter is the shoulder on the low frequency side of the PO_2^- symmetric stretch at 1095 cm^{-1}).[50–52]

Seawater and the sea-salt particles derived from it contain a number of minor components in addition to NaCl.[34,35] These include hygroscopic salts such as those of magnesium (molar ratio of Na^+ to Mg^{2+} = 8.9 : 1) as well as infrared-active species such as sulfate (molar ratio $Cl^-:SO_4^{2-}$ = 19:1) and bicarbonate (molar ratio $Cl^-:HCO_3^-$ = 260 : 1).[34,35] As a result, the spectrum of IO alone (bottom spectrum, Fig. 1b) shows peaks due to sulfate (1050–1250 cm^{-1} region) and bicarbonate (~1420 cm^{-1}). The salts that are hygroscopic not only adsorb water on their surface during sample preparation, but also exist in the form of hydrates such as $MgCl_2{\cdot}6H_2O$.[34,40] As a result, several peaks due to the water bending vibration (in the 1600–1660 cm^{-1} region) and to the O–H stretch (in the 3000–3800 cm^{-1} region) appear in the spectrum. Because of the strong absorptions due to water and other components of IO, the peaks from the relatively small amounts of POPC are not as distinct as on NaCl. The same is true for POPC/$MgCl_2{\cdot}6H_2O$/NaCl mixtures (not shown) where water also dominates the spectrum.

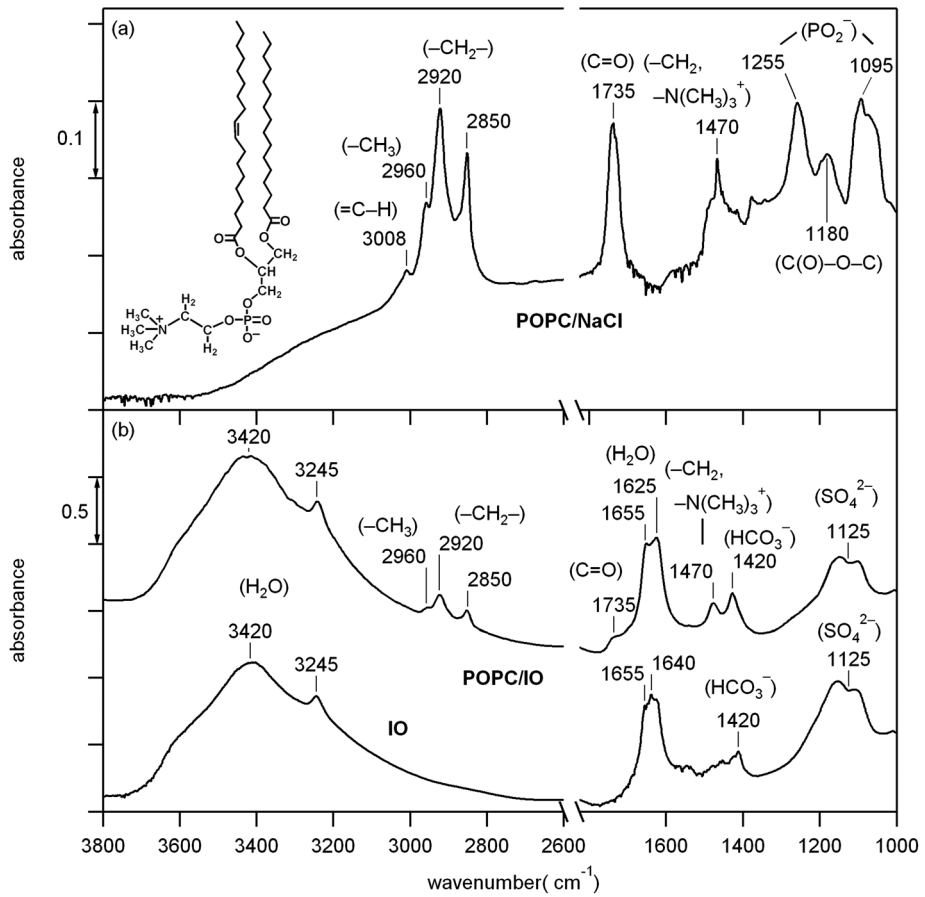

Fig. 1 DRIFTS spectra of (a) POPC/NaCl, (b) POPC/IO (top) and IO (bottom). Absorbance is calculated as $\log_{10}(S_0/S_1)$ where S_0 is the single beam spectrum of NaCl and S_1 is the single beam spectrum of the sample. The structure of POPC is shown in (a).

Despite these strong overlapping absorptions due to the substrate, changes in POPC upon reaction with gas phase ozone can be readily followed with time by using the single beam spectrum just before reaction as the reference. This allows small changes in the presence of a large ''background'' to be followed quantitatively, as has been done for example, for the oxidation of self-assembled monolayers.[53–56] Fig. 2 shows typical changes in the infrared spectra for POPC/IO and POPC/$MgCl_2{\cdot}6H_2O$/NaCl as a function of time upon reaction with 1.2×10^{13} O_3 cm^{-3}. As expected, there is a decrease in the 3008 cm^{-1} band due to loss of H–C═C. In addition, absorptions due to $-CH_2-$ groups (2920 and 2850 cm^{-1}) decrease.

Ozone reacts with the double bond in POPC *via* the Criegee mechanism (Scheme 1).[57–60] In the gas phase, the Criegee intermediates (CI) are formed with excess energy and can decompose, or be collisionally stabilized and react further with such species as water or aldehydes.[59–66] When the reaction occurs in/on a condensed phase as in the present studies, the CI would be expected to be stabilized to a much greater extent than in the gas phase. As discussed in more detail below, the smaller fragments such as nonanal would be expected to be sufficiently volatile to be removed in the gas stream, leading to loss of $-CH_2-$ groups as observed.

During the reaction, new bands are observed during the reaction at 1743 and 1710 cm^{-1} (Fig. 2). These are assigned to non-hydrogen bonded carboxylic acids (1743 cm^{-1}) and aldehyde and/or hydrogen bonded carboxylic acids (1710 cm^{-1}), respectively.[50] New product peaks also appear at 2950, 2880, 1385, and 1110 cm^{-1}, and are assigned to a secondary ozonide (SOZ).[28,50,54,67–73] The band at 1110 cm^{-1} in the Instant Ocean spectra (Fig. 2a) is largely obscured by small changes in the strong sulfate band in that region (Fig. 1b). Changes at 2950 cm^{-1} and 2880 cm^{-1} were also observed in studies on ozonolysis of OPPC/NaCl.[28] These changes were assigned to H–C stretches of the ring carbons of the SOZ. In some studies of alkene ozonolysis on surfaces, new bands in this region were assigned to methyl groups,[74–76] but the spectral region that carries the characteristic C–O stretch of the SOZ at lower wavenumbers was not experimentally accessible in those studies. The simultaneous formation of

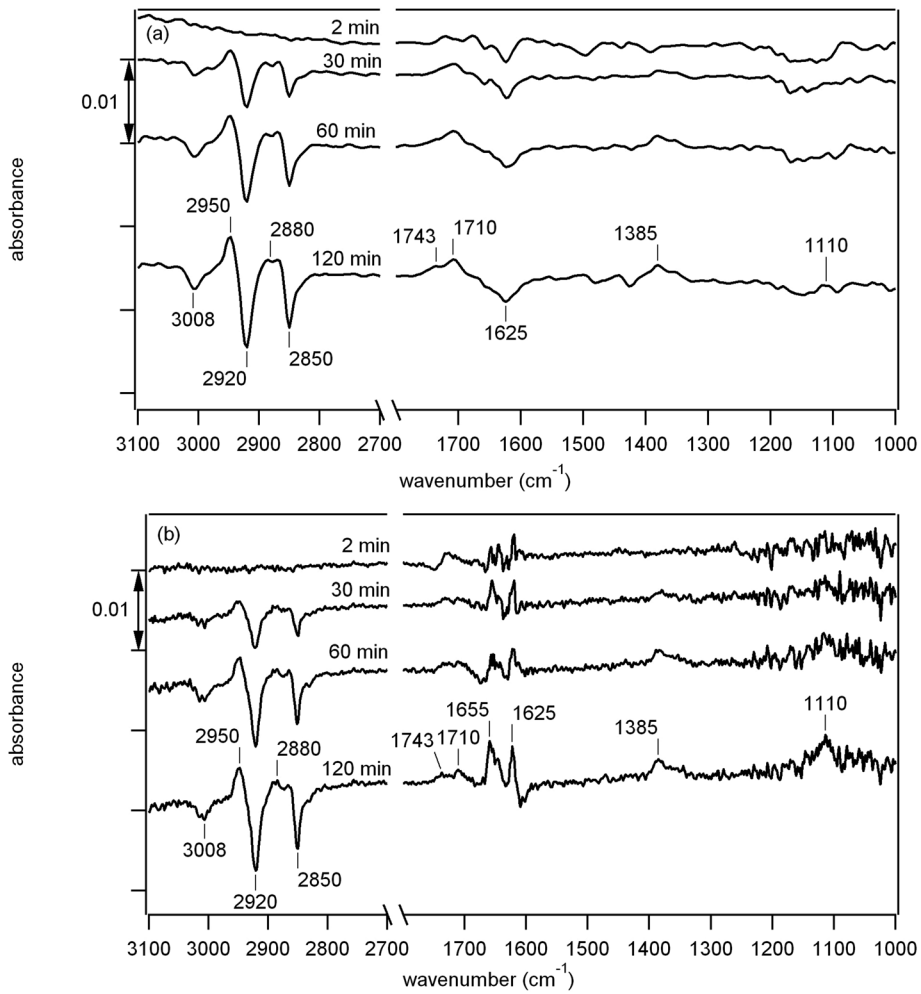

Fig. 2 DRIFTS spectra of (a) POPC/IO and (b) POPC/$MgCl_2{\cdot}6H_2O$/NaCl during reaction with 1.2×10^{13} O_3 cm^{-3}. Absorbance is calculated as $\log_{10}(S_1/S_n)$ where S_1 is the single beam spectrum of unreacted POPC/IO or POPC/$MgCl_2{\cdot}6H_2O$/NaCl and S_n is the single beam spectrum of POPC/IO or POPC/$MgCl_2{\cdot}6H_2O$/NaCl reacted for n minutes.

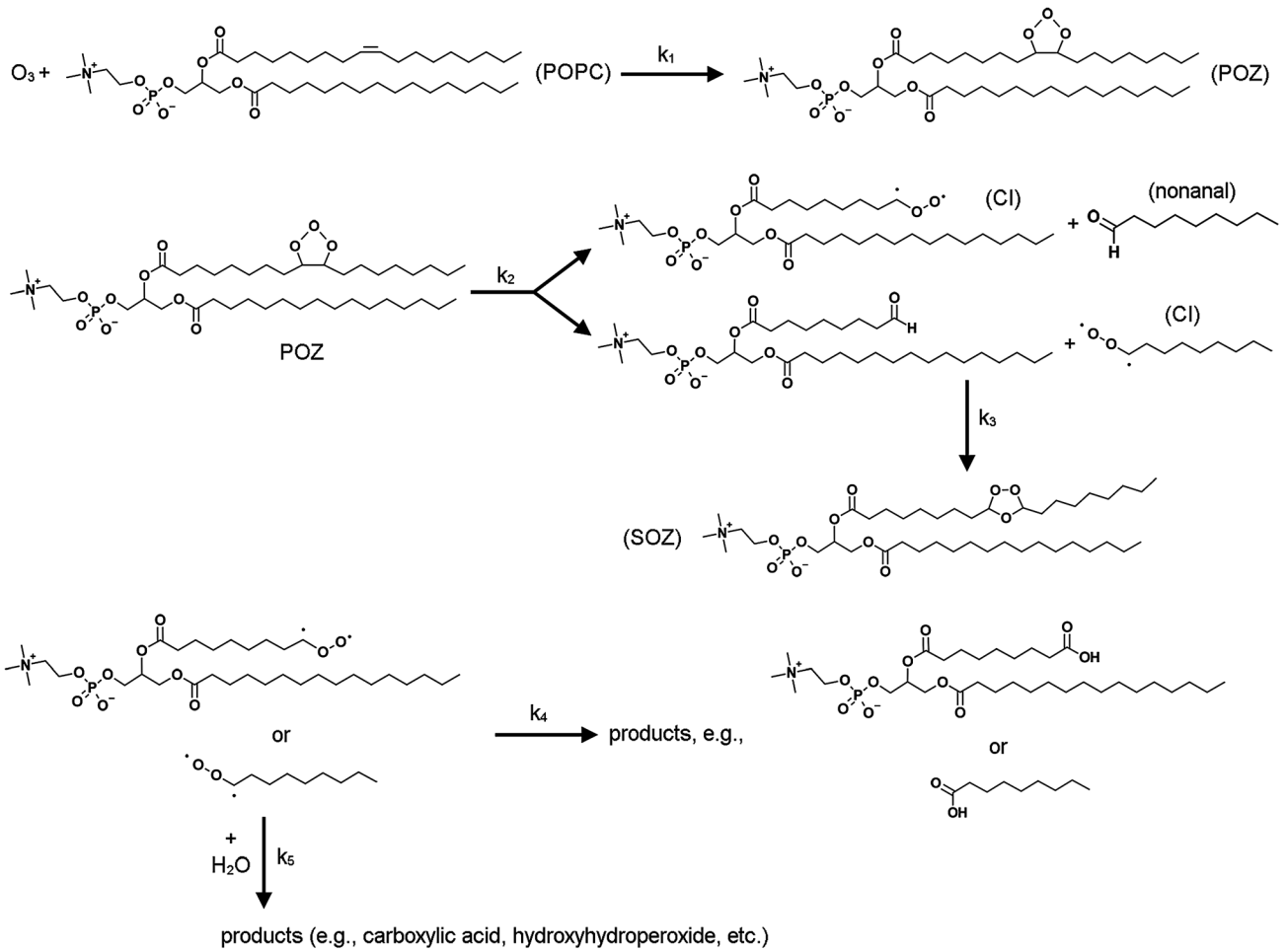

Scheme 1 Criegee mechanism for the reaction of O_3 with POPC.

bands 1110 and 1385 cm^{-1} that increased in proportion to the 2950 and 2880 cm^{-1} bands provides strong support for their assignment to SOZ in the present case.

Further support for identification of these products comes from the MALDI-TOF mass spectra which are similar to those reported earlier for the oxidation of unsaturated phosphocholines.[28,42,70,77] Thus, after reaction, peaks expected from the phospholipid aldehyde at m/z 650.4 $[RCHO + H]^+$ and m/z 672.4 $[RCHO + Na]^+$, the corresponding carboxylic acid at m/z 666.4 $[RCOOH + H]^+$ and m/z 688.4 $[RCOOH + Na]^+$, and the secondary ozonide at m/z 808.6 $[SOZ + H]^+$ are observed.

The change in intensity of the $-CH_2-$ bands at 2920 and 2850 cm^{-1} can be used to examine the distribution of major products. If all of the CI and aldehyde formed simultaneously recombined to form SOZ (Scheme 1), no loss of $-CH_2-$ and hence no change in the bands at 2920 and 2850 cm^{-1} would be observed. However, if this recombination is not 100% efficient and the 9-carbon compounds formed from scission of the double bond are volatile, they will be removed from the surface into the gas stream, which is not detectable by DRIFTS. This would result in loss of intensity at 2920 and 2850 cm^{-1}, as is observed. In the extreme case that all of the C_9 fragments were pumped away, seven out of 32 $-CH_2-$ groups in each POPC molecule would be lost, and the bands at 2920 and 2850 cm^{-1} would decrease in intensity by 7/32 of the initial value. The fractional loss of $-CH_2-$ groups can therefore be used to estimate the branching ratio for reactions (4) + (5) in Scheme 1 compared to reaction (3) to form SOZ:

$$\frac{k_4 + k_5[H_2O]}{k_3[RCHO] + k_4 + k_5[H_2O]} = \frac{\left(\frac{\Delta A}{A_{initial}}\right)_{average}}{\left(\frac{7}{32}\right)} \qquad (I)$$

In eqn (I), ΔA is the change in absorbance of $-CH_2-$ at 2850 or 2920 cm^{-1} at the end of the reaction, $A_{initial}$ is the corresponding initial absorbance and their ratio represents the fractional loss of $-CH_2-$ groups. For POPC/IO, the fractional loss of $-CH_2-$ groups averaged over the 2920 and 2850 cm^{-1} bands was 0.10 ± 0.02 (1s), which gives a branching ratio from eqn (I) of 0.45 ± 0.11 (1s). That is, 45% of the ozonolysis of POPC on IO results in C=C bond scission and loss of the C_9 fragment, implying that the remaining 55% gives SOZ. For POPC/$MgCl_2 \cdot 6H_2O$/NaCl, the fractional loss of $-CH_2-$ groups averaged over the 2920 and 2850 cm^{-1} bands was 0.11 ± 0.02 (1s), which gives a branching ratio of 0.50 ± 0.10 (1s), *i.e.*, half of the reaction forms fragments and the other half SOZ. In short, the branching ratio is the same within experimental error for both substrates, 0.5 ± 0.1 (1s).

This analysis assumes that the C_9 products are removed from the surface. In studies of the oxidation of the analogous OPPC on a water subphase, it was shown using authentic samples of gas phase nonanal that about half of the aldehyde generated in the reaction was taken up into the aqueous subphase.[43] While there is water on the salt in the present studies, it is not expected to be nearly as efficient in nonanal uptake as liquid water, particularly given the lowering of organic solubilities due to the salting out effect.[78] Hence on the synthetic sea salt used here, the assumption that nonanal does not remain on the salt is reasonable. Nonanoic acid, however, has been observed to remain in the condensed phase upon ozonolysis of oleic acid or sodium oleate particles.[79,80] Since this analysis assumes that all C_9 fragments formed are removed from the salt, it gives a lower limit for the branching ratio for reactions (4) + (5), and hence an upper limit of $\sim$50% for reaction (3) to form SOZ. However, in one experiment, air was left flowing over the sample after oxidation; no change in the negative peaks at 2920 and 2850 cm^{-1} was observed over the course of an hour, suggesting products on the salt were not volatile.

Kinetics

The ozone concentration remains constant in these experiments because the ozone–air mixture is flowing through the sample and is continually refreshed. The initial rate of loss of POPC is given by eqn (II),

$$-\left(\frac{d[POPC]}{dt}\right)_{t=0} = k_1[O_3]_0[POPC]_0 \qquad (II)$$

where k_1 is the rate constant for reaction (1) and $[POPC]_0$ and $[O_3]_0$ are the initial reactant concentrations. The concentration of O_3 remains constant in the flow over the POPC/salt during the experiments, so that $[O_3]_0 = [O_3]_t$ at all times. Because it is difficult to quantitatively extract small changes in the H–C=C signal at 3008 cm^{-1}, using this peak to follow the kinetics is not feasible. As an alternative, the formation of the product SOZ which has relatively strong bands at 2950 and 2880 cm^{-1} was used to extract the rate constant based on the reactions in Scheme 1.

If POZ and CI are in steady-state, their concentrations are given by eqn (III) and (IV) respectively:

$$[POZ]_{ss} = \frac{k_1[O_3]_0[POPC]}{k_2} \qquad (III)$$

$$[CI]_{ss} = \frac{k_2[POZ]_{ss}}{k_3[RCHO] + k_4 + k_5[H_2O]} = \frac{k_1[O_3]_0[POPC]}{k_3[RCHO] + k_4 + k_5[H_2O]} \qquad (IV)$$

The rate of SOZ formation is then given by:

$$\frac{d[SOZ]}{dt} = k_3[CI]_{ss}[RCHO] = k_1[O_3]_0[POPC]\frac{k_3[RCHO]}{k_3[RCHO] + k_4 + k_5[H_2O]} \qquad (V)$$

The ratio $k_3[RCHO]/(k_3[RCHO] + k_4 + k_5[H_2O])$ is the branching ratio for the formation of SOZ (BR^{SOZ}). At short reaction times ($t \rightarrow 0$), [POPC] is the initial concentration, $[POPC]_0$. Assuming that the branching ratio is constant over the course of the experiment, eqn (V) becomes

$$\left(\frac{d[SOZ]}{dt}\right)_{t=0} = k_1[O_3]_0[POPC]_0(BR^{SOZ}) \qquad (VI)$$

The initial rate of SOZ formation can be obtained using the absorbance at 2950 cm^{-1} and the final SOZ absorbance at long reaction times as a reference. Because this peak is overlapped by the negative peak due to loss of $-CH_2-$ groups, the corrected absorbance due to SOZ was obtained by adding back a fraction of the initial POPC/salt spectrum until the negative absorption from $-CH_2-$ at 2920 cm^{-1} was cancelled out. This allowed the absorbance of the 2950 cm^{-1} SOZ peak to be quantified to obtain the rate of formation of SOZ:

$$\left(\frac{d[SOZ]}{dt}\right)_{t=0} = \left(\frac{dA_{2950}}{dt}\right)_{t=0} \times \frac{[SOZ]_\infty}{(A_{2950})_\infty} \qquad (VII)$$

$[SOZ]_\infty$ and $(A_{2950})_\infty$ are the SOZ concentration and its absorbance at the end of the reaction. Assuming that all of the C=C in the POPC reacts, which is reasonable for most experiments as discussed below, then $[SOZ]_\infty = (BR^{SOZ})[POPC]_0$. Using this with eqn (VI) and (VII) gives the relationship between the SOZ absorbance at 2950 cm^{-1} and the rate constant k_1:

$$\left(\frac{dA_{2950}}{dt}\right)_{t=0} \times \frac{1}{(A_{2950})_\infty} = k_1[O_3]_0 \qquad (VIII)$$

Fig. 3 shows SOZ peak intensities at 2950 cm^{-1} as a function of reaction time and at four different ozone concentrations for typical experiments, normalized for the initial amount of POPC by dividing by the initial absorbance of $-CH_2-$ groups at 2850 cm^{-1}. The final SOZ absorbance ratio at long reaction times for POPC/$MgCl_2 \cdot 6H_2O$/NaCl (Fig. 3b) trends to a common value of $\sim$0.15 at all ozone concentrations, as expected for complete reaction of POPC. However, for POPC/IO (Fig. 3a), this is only true at higher ozone concentrations. A potential reason for this difference is that not all of the POPC double bonds are available for reaction on IO, but they are on $MgCl_2 \cdot 6H_2O$.

The major difference between these substrates is in their hygroscopicity. Magnesium chloride is more hygroscopic. For example, this salt was observed to deliquesce readily in room air, whereas IO does not. Thus, even without added water vapor, one might expect the surface POPC film to be more liquid-like than on IO. This fluidity should enhance the accessibility of the double bond to incoming gases, as suggested by molecular dynamics simulations.[81] To test this, experiments were carried out in which water vapor was also present at relative humidities up to 1.4×10^{17} molecules H_2O cm^{-3} (20% RH) at an ozone concentration of 3.9×10^{13} O_3 cm^{-3} (1.6 ppm). Adding water vapor has an effect on reactions in other systems,[82] but in this case, as discussed above, water is already present on the samples because of the hygroscopic nature of the salts. Adding water vapor increases the ''background'' on which changes in POPC occur. However, differences are still observed between experiments in dry air and those with added water vapor. Fig. 4 shows typical spectra, normalized for the initial amount of POPC, of (a) POPC/IO and

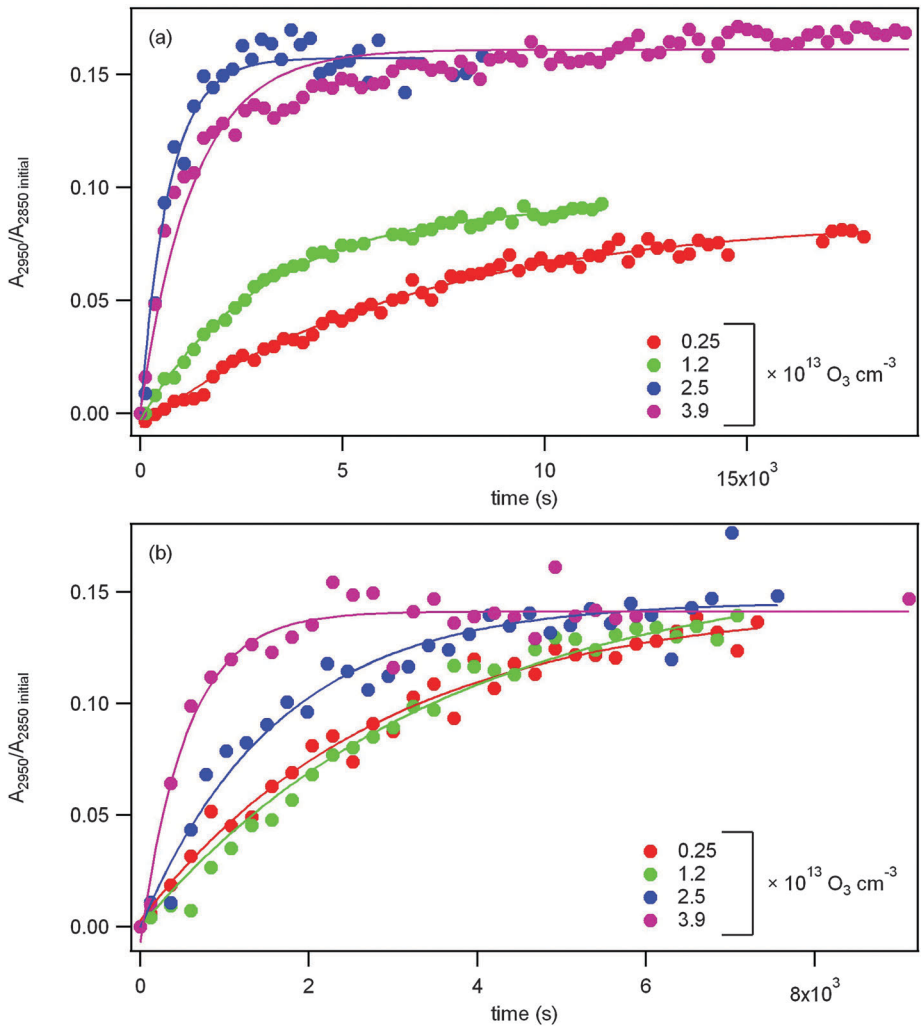

Fig. 3 Absorbance of SOZ at 2950 cm^{-1} normalized to the initial amount of POPC using the 2850 cm^{-1} band as a function of reaction time with various ozone concentrations for (a) POPC/IO and (b) POPC/$MgCl_2$·$6H_2O$/NaCl. The lines are exponential fits to each data set.

(b) POPC/$MgCl_2$·$6H_2O$/NaCl after 58 minutes of reaction without added water vapor (top) and at 0.68 × 10^{17} molecules H_2O cm^{-3} (10% RH) (bottom). For both salt substrates, the relative loss of –CH_2– groups is greater and the increase in the SOZ bands at 2950 and 2880 cm^{-1} is smaller at 0.68 × 10^{17} molecules H_2O cm^{-3} (10% RH), indicating that less SOZ and more volatile aldehydes and/or carboxylic acid products are formed. Furthermore, there is now only one peak at 1743 cm^{-1} in the C═O region, consistent with increased reaction of CI with water to give non-hydrogen bonded carboxylic acid products.

To examine the change in SOZ relative to the alternate channels that generate acid and aldehyde (Scheme 1), changes in the SOZ absorbance at 2950 cm^{-1} and in –CH_2– groups at 2850 cm^{-1} (representing the formation of volatile products) were quantified. This provides a measure of $\Delta[SOZ]/\Delta[C_9]_{volatile}$, where $\Delta[C_9]_{volatile}$ represents C_9 products such as nonanal that do not remain on the salt and hence are not detected by DRIFTS. Fig. 5 shows this ratio as a function of water vapor concentration at long reaction times where $A_{2950} = (A_{2950})_\infty$. There is a large decrease in $\Delta[SOZ]/\Delta[C_9]_{volatile}$ from 0 to 0.34 × 10^{17} molecules H_2O cm^{-3} (5% RH), with relatively little change as the water vapor concentration is increased further. The shape of these curves is determined primarily by the decrease in the SOZ absorbance, with much smaller changes due to –CH_2–. This suggests that even relatively small amounts of water vapor are sufficient to trap at least some of the Criegee intermediate, decreasing the SOZ yield. The smaller change in the –CH_2– loss suggests that increasing amounts of the C_9 products are retained on the salt surface as the water vapor concentration increases, which is expected particularly for acids which tend to be relatively "sticky" as well as more soluble than aldehydes. As mentioned above, retention of product carboxylic acids in the condensed phase has been reported, for example, in the ozonolysis of oleic acid or sodium oleate particles.[79,80]

A decrease in the amount of SOZ formed and increase in carbonyl compounds, especially carboxylic acids, with added water vapor has been observed previously for ozonolysis of unsaturated phospholipids on NaCl.[28] While carboxylic acids

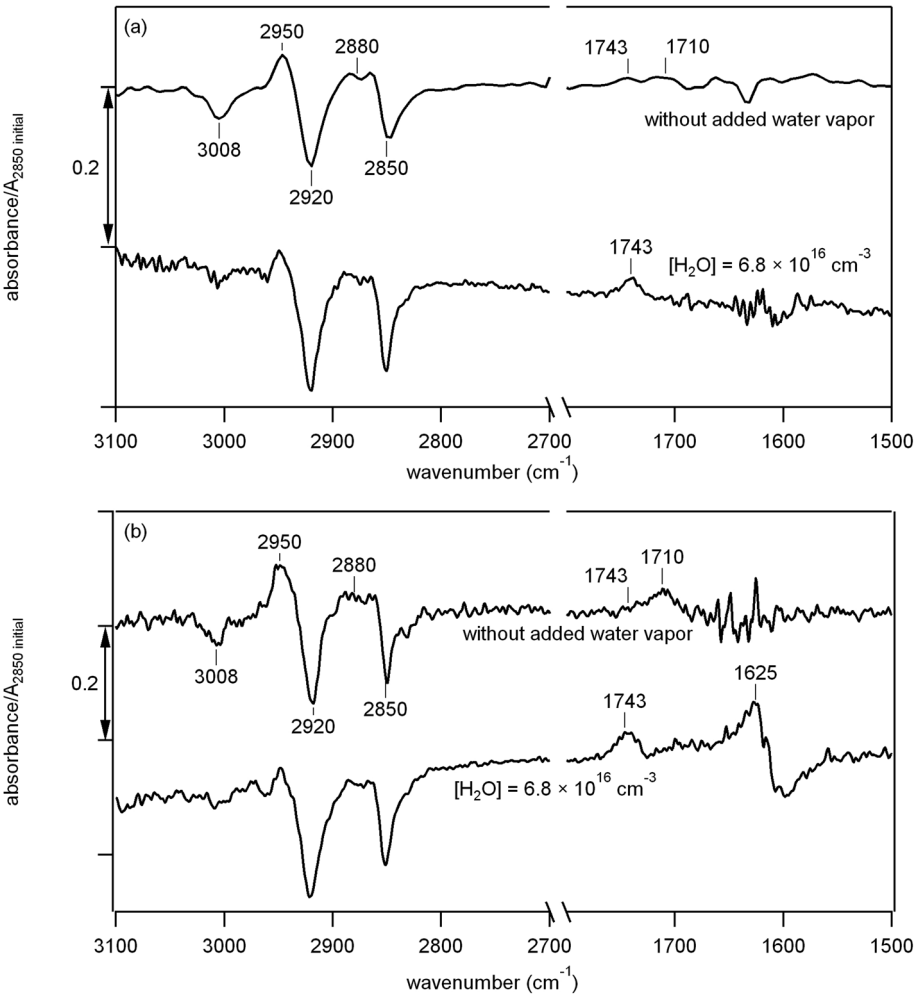

Fig. 4 DRIFTS spectra of (a) POPC/IO and (b) POPC/$MgCl_2$·$6H_2O$/NaCl after 58 minutes of reaction with 3.9×10^{13} O_3 cm^{-3} either without added water vapor or with 6.8×10^{16} molecules cm^{-3} (10% RH) added water vapor. Spectra were normalized by dividing by the initial value of A_{2850} for each spectrum. Absorbance is calculated as $\log_{10}(S_1/S_{58})$ where S_1 is the single beam spectrum of POPC/IO or POPC/$MgCl_2$·$6H_2O$/NaCl just prior to reaction and S_{58} is the single beam spectrum of POPC/IO or POPC/$MgCl_2$·$6H_2O$/NaCl after 58 minutes reaction time.

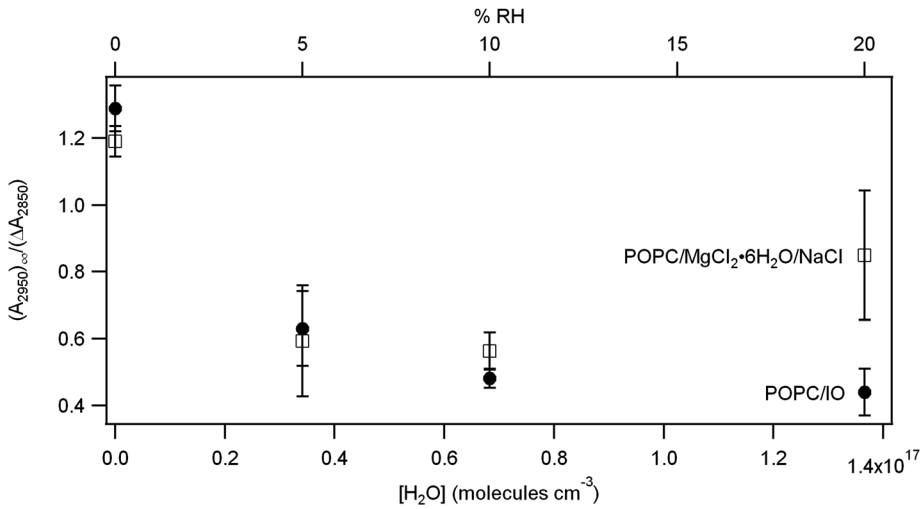

Fig. 5 Absorbance of SOZ at 2950 cm^{-1} at the longest reaction times divided by the absolute change in the absorbance of $-CH_2-$ at 2850 cm^{-1} as a function of water concentration for POPC/IO (filled circles) and POPC/$MgCl_2$·$6H_2O$/NaCl (open squares).

are formed in the absence of water *via* isomerization of the CI,[59,60,62,83] they are also known to be formed in the reaction of CI with water.[59,60,62,64,65,84,85] The increase in acids and decrease in SOZ are thus consistent with known ozonolysis reactions. The reaction of the CI with water is also known to form hydroxyhydroperoxides which can decompose to generate aldehydes and hydrogen peroxide.[61,64,86–93]

Adding water vapor to the gas stream may not only affect the product distribution but also the kinetics if it affects the fluidity of the POPC film on the surface. This is consistent with the increase in $[SOZ]_\infty$ with $[O_3]_0$ for POPC on IO but not on magnesium chloride. Thus, if the latter already holds sufficient surface water that the POPC on the surface behaves like a dynamic, fluid film, then the double bonds will be more readily accessible under all reaction conditions. However, on the less hygroscopic IO in the absence of added water vapor, this is not the case. Addition of water vapor to POPC/IO increases the fluidity of the film and availability of C=C for reaction. This is supported by the observation that the *rates* of formation of SOZ increase with water vapor on IO (Fig. 6), although the relative yield of SOZ decreases when water vapor is added (Fig. 5). That is, gaseous water increases the availability of the double bond for reaction and hence the rate of product formation, but also impacts the chemistry by intercepting the Criegee intermediate, lowering the SOZ yield. While the relative yield of SOZ decreases with water vapor for the magnesium chloride substrate (Fig. 5) as well, the trend in the rates of SOZ formation with water vapor concentration was smaller than that for IO (Fig. 6), consistent with the greater fluidity of the film and greater availability of the double bond.

The fact that SOZ is still observable at 1.4×10^{17} molecules H_2O cm^{-3} (20% RH) shows that the CI is not completely trapped by water, and some CI can still recombine with the aldehyde. Similar observations were made for the ozonolysis of POPC liposomes in aqueous solution[94] and methyl oleate in aqueous micelles of sodium dodecyl sulfate[95] where the yields of SOZ were 11%, compared to 89% for the methyl oleate reaction in hexane. SOZ production was also observed in the reaction of O_3 with 1-palmitoyl-2-oleoyl-*sn*-phosphatidylglycerol surfactant on a 1 : 1 water–methanol solution.[93]

A similar and even more dramatic effect on the final SOZ yield was seen in earlier studies on NaCl where the rate of SOZ formation increased with O_3 and the SOZ yield decreased with added water vapor.[28] In this case where there is very little water vapor on the surface and the POPC will not be a fluid film, the ozone reaction itself may cause disruption of the arrangement of surface POPC by reacting with those double bonds that are accessible. Loss of C_9 fragments would result in increased disorder, making new double bonds more accessible to ozone. The effect would be expected to be largest at the highest ozone concentrations, as observed. This suggests that a similar effect may also be at work for POPC/IO. Support for such an effect comes from studies of phospholipid monolayers in which oxidation disrupted the structure of the monolayer.[96,97] In a related system, oxidation of phospholipid bilayers with scission at the C=C bond was also predicted to disrupt the structure, forming pores and increasing permeability.[98–101]

Eqn (VIII) predicts that plots of $(dA_{2950}/dt) \times (1/A_{2950})_\infty$ *versus* $[O_3]_0$ should be linear, consistent with the data shown in Fig. 7. The values obtained for k_1 from the slopes of the least squares lines for the two substrates are the same within experimental error (1s), $k_1 = (4 \pm 1) \times 10^{-17}$ cm^3 $molecule^{-1}$ s^{-1} for POPC/IO and $k_1 = (3.4 \pm 0.7) \times 10^{-17}$ cm^3 $molecule^{-1}$ s^{-1} (1s) for POPC/$MgCl_2$·$6H_2O$/NaCl. Note that the systematic error associated with the value for the POPC/IO will be larger due to the lack of full availability of the double bonds for reaction at lower ozone concentrations. Despite this, the least squares line for POPC/IO in Fig. 7 has an intercept very close to 0.

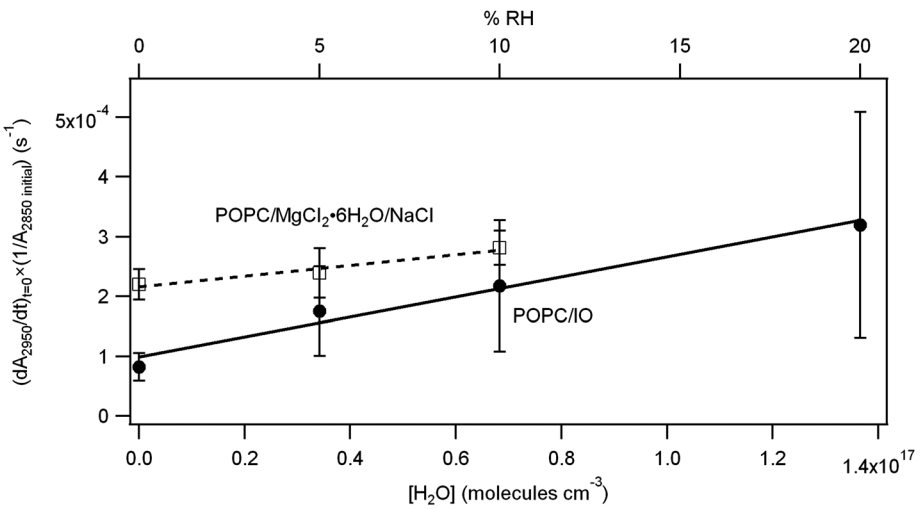

Fig. 6 Initial rate of change of absorbance at 2950 cm^{-1} of SOZ normalized to the initial absorbance of $-CH_2-$ at 2850 cm^{-1} as a function of water vapor concentration in the reaction of 3.9×10^{13} O_3 cm^{-3} with POPC/IO (filled circles, solid line) and POPC/$MgCl_2$·$6H_2O$/NaCl (open squares, dashed line). $(dA_{2950}/dt)_{t=0}$ is given by the slope at $t = 0$ of exponential fits to A_{2950} *vs.* time plots. The data are weighted averages of 2–4 experiments with 1s error bars. No data are shown for POPC/$MgCl_2$·$6H_2O$/NaCl at 1.4×10^{17} molecules H_2O cm^{-3} (20% RH) because of problems with obtaining reproducible data for this system at this relatively high water vapor concentration.

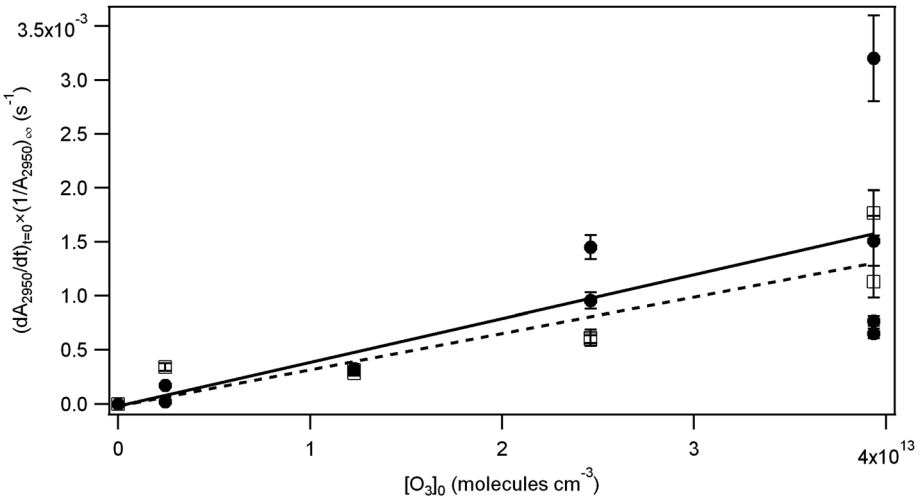

Fig. 7 Initial rate of change of absorbance at 2950 cm^{-1} due to SOZ divided by the value of A_{2950} at infinite time as a function of ozone concentration for reaction with POPC/IO (filled circles, solid line) and POPC/$MgCl_2 \cdot 6H_2O$/NaCl (open squares, dashed line). $(dA_{2950}/dt)_{t=0}$ is given by the slope at $t = 0$ of exponential fits to A_{2950} *vs.* time plots. Error bars are 1s obtained by propagating the errors from the exponential fits; scatter is from systematic error.

From collision theory, the reaction probability (γ) is related to the loss of POPC by[59]

$$\#\text{POPC}\,\text{cm}^{-2}\,\text{s}^{-1} = \gamma[\text{O}_3]_0\sqrt{\frac{RT}{2\pi \text{M}_{\text{O}_3}}} \qquad \text{(IX)}$$

where R is the gas constant, T is the temperature (K), and M_{O_3} is the molar mass of ozone. The left side of eqn (IX) can be obtained from eqn (II) assuming a surface concentration of POPC[28] of 1.6×10^{14} molecules cm^{-2} and the values derived above for k_1. This gives $\gamma = (7 \pm 3) \times 10^{-7}$ (1s) on the IO substrate and $\gamma = (6 \pm 1) \times 10^{-7}$ (1s) for magnesium chloride/NaCl. Given the experimental challenges, small signals and quantitative reproducibility from run to run (Fig. 7), we estimate the overall uncertainty in the reaction probabilities is a factor of two.

In previous studies of ozonolysis of a monolayer of POPC on liquid water, lower limits for the reaction probabilities of $\gamma \geq (3\text{–}4) \times 10^{-6}$ were reported[42,43] and a corrected value on solid NaCl[28] is $\gamma = (3\text{–}6) \times 10^{-8}$. As discussed earlier, the amount of water present in the system affects the accessibility of the double bond and hence the reaction probability. The trend in reaction probability with water vapor concentration supports this interpretation in that the reaction is faster when the phospholipid is spread as a fluid film on water.

Atmospheric implications

Sea-salt particles under most atmospheric conditions will be liquid.[102] Although the deliquescence and efflorescence relative humidities at 298 K of the major component, NaCl, are 75% and 44% respectively,[48,103–105] sea salt contains a number of other, more hygroscopic components such as magnesium chloride. As a result, sea-salt particles remain liquid to much lower relative humidities than pure NaCl.[106,107] The most relevant model for reactions of organic layers, including biologically-derived materials such as phosphocholines, on sea-salt particles may thus be an organic film on a core of a liquid salt solution. In this case, reaction probabilities for O_3 with the double bond equal to 3×10^{-6} or greater[42,43] are appropriate.

In some circumstances, however, sea-salt particles may be more solid-like. For example, recent studies of mixed organic–aqueous inorganic particles suggest that the organic portion may be phase-separated from the aqueous component.[36–39] Organics on such particles may behave more like POPC on the substrates used in the present studies. In this case, a reaction probability of 6×10^{-7} should be applicable, giving a predicted lifetime of POPC of 3 hours for an ozone concentration of 2.5×10^{12} molecules cm^{-3} (100 ppb). The lifetime will be much shorter, ~30 min or less, if the POPC forms a fluid coating on a liquid substrate. During the daytime, sunlight will induce additional chemistry due to OH formation and halogen activation.[108,109]

Conclusions

These studies show that the reactivity and products of oxidation of unsaturated phospholipids on sea-salt particles in air will be very sensitive to the nature of the substrate, particularly its phase, the availability of water and whether there is phase separation between the organic and the salt mixture. In all cases, 1-palmitoyl-2-oleoyl-*sn-glycero*-3-phosphocholine (POPC), a component of biological systems, will be readily oxidized by gas phase ozone when it is present on the surface of sea-salt particles. The models for sea salt used here, a commercially available salt mixture and $MgCl_2 \cdot 6H_2O$/NaCl, are hygroscopic and retain water under mild pumping. The presence of water associated with the salts affects the product distribution from the ozonolysis, with the yield of the SOZ falling to $\leq 50\%$ compared to much higher SOZ yields for NaCl as a substrate.[28] The addition of water vapor further decreases the branching

ratio for the CI reaction to generate SOZ on both substrates. Water vapor is also shown to affect the absolute rate of SOZ formation, particularly on the less hygroscopic commercial sea salt. This is attributed to increasing fluidity of the POPC on the surface, thus enhancing the availability of the double bond to the gas phase. Reaction probabilities on both substrates are $\sim 6 \times 10^{-7}$, smaller than previously measured for similar phospholipids on aqueous substrates. Which of the model substrates, solids or aqueous solutions, is most relevant for atmospheric reactions will depend on the particular conditions and particle morphology.

Acknowledgements

This work was supported by the National Science Foundation (Grant No. 0836735 and 1207112). The authors would like to thank John Greaves, Theresa McIntire, Lisa Wingen, Samar Moussa, and Nicole Richards for helpful discussions, and James N. Pitts Jr. for helpful discussions and comments on the manuscript.

References

1 E. R. Lewis and S. E. Schwartz, *Sea Salt Aerosol Production: Mechanisms, Methods, Measurements and Models. A Critical Review*, American Geophysical Union, Washington, D.C., 2005.
2 A. H. Woodcock, *J. Meteorol.*, 1953, **10**, 362–371.
3 A. H. Woodcock, *J. Geophys. Res.*, 1972, **77**, 5316–5321.
4 D. C. Blanchard, *J. Geophys. Res.*, 1985, **90**, 961–963.
5 D. M. Murphy, *et al.*, *Nature*, 1998, **392**, 62–65.
6 IPCC, *Climate Change 2007: The Physical Science Basis. Contribution of Working Group I to the Fourth Assessment Report of the Intergovernmental Panel on Climate Change*, Cambridge University Press, Cambridge, U.K., 2007.
7 M. O. Andreae and D. Rosenfeld, *Earth-Sci. Rev.*, 2008, **89**, 13–41.
8 Y. Rudich, N. M. Donahue and T. F. Mentel, *Annu. Rev. Phys. Chem.*, 2007, **58**, 321–352.
9 L. Smoydzin and R. von Glasow, *Atmos. Chem. Phys.*, 2007, **7**, 5555–5567.
10 P. S. Gill, T. E. Graedel and C. J. Weschler, *Rev. Geophys. Space Phys.*, 1983, **21**, 903–920.
11 D. C. Blanchard, *Estuaries*, 1989, **12**, 127–137.
12 G. B. Ellison, A. F. Tuck and V. Vaida, *J. Geophys. Res.*, 1999, **104**, 11633–11641.
13 D. J. Donaldson and V. Vaida, *Chem. Rev.*, 2006, **106**, 1445–1461.
14 J. C. Marty, A. Saliot, P. Buatmenard, R. Chesselet and K. A. Hunter, *J. Geophys. Res.*, 1979, **84**, 5707–5716.
15 R. B. Gagosian, E. T. Peltzer and O. C. Zafiriou, *Nature*, 1981, **291**, 312–315.
16 B. Alberts, D. Bray, J. Lewis, M. Raff, K. Roberts and J. D. Waston, in *Molecular Biology of the Cell*, Garland, New York, 1989, chap. 6.
17 J. M. Prospero, in *Chemistry of Marine Water and Sediments*, ed. A. Gianguzza, E. Pellizzetti and S. Sammarano, Springer-Verlag, Berlin, 2002, pp. 35–82.
18 H. Tervahattu, K. Hartonen, V. M. Kerminen, K. Kupiainen, P. Aarnio, T. Koskentalo, A. F. Tuck and V. Vaida, *J. Geophys. Res.*, 2002, **107**, DOI: 10.1029/2000JD000282.
19 H. Tervahattu, J. Juhanoja and K. Kupiainen, *J. Geophys. Res.*, 2002, **107**, DOI: 10.1029/2001JD001403.
20 P. K. Quinn and T. S. Bates, *Nature*, 2011, **480**, 51–56.
21 T. S. Bates, *et al.*, *J. Geophys. Res.*, 2012, **117**, DOI: 10.1029/2012jd017588 D00v15.
22 C. D. O'Dowd, M. C. Facchini, F. Cavalli, D. Ceburnis, M. Mircea, S. Decesari, S. Fuzzi, Y. J. Yoon and J. P. Putaud, *Nature*, 2004, **431**, 676–680.
23 M. C. Facchini, *et al.*, *Geophys. Res. Lett.*, 2008, **35**, 5.
24 K. E. Broekhuizen, T. Thornberry, P. P. Kumar and J. P. D. Abbatt, *J. Geophys. Res.*, 2004, **109**, DOI: 10.1029/2004JD005298.
25 S. J. Ghan and S. E. Schwartz, *Bull. Am. Meteorol. Soc.*, 2007, **88**, 1059–1083.
26 J. Zahardis and G. A. Petrucci, *Atmos. Chem. Phys.*, 2007, **7**, 1237–1274.
27 V. N. Bochkov, O. V. Oskolkova, K. G. Birukov, A. L. Levonen, C. J. Binder and J. Stockl, *Antioxid. Redox Signaling*, 2010, **12**, 1009–1059.
28 F. Karagulian, A. S. Lea, C. W. Dilbeck and B. J. Finlayson-Pitts, *Phys. Chem. Chem. Phys.*, 2008, **10**, 528–541.
29 M. P. Fuller and P. R. Griffiths, *Am. Lab.*, 1978, **10**, 69.
30 M. P. Fuller and P. R. Griffiths, *Anal. Chem.*, 1978, **50**, 1906–1910.
31 P. R. Griffiths and M. P. Fuller, in *Advances in Infrared and Raman Spectroscopy*, ed. R. J. H. Clark and R. E. Hester, Heyden and Sons, London, 1982, vol. 9, pp. 63–129.
32 R. Vogt and B. J. Finlayson-Pitts, *J. Phys. Chem.*, 1994, **98**, 3747–3755.
33 L. I. Nieto-Gligorovski, S. Net, S. Gligorovski, H. Wortham, H. Grothe and C. Zetzsch, *Atmos. Environ.*, 2010, **44**, 5451–5459.
34 D. R. Kester, I. W. Duedall, D. N. Connors and R. M. Pytkowicz, *Limnol. Oceanogr.*, 1967, **12**, 176.
35 M. J. Atkinson and C. Bingman, *J. Aquaric. Aquat. Sci.*, 1997, **8**, 39–43.
36 A. K. Bertram, *et al.*, *Atmos. Chem. Phys.*, 2011, **11**, 10995–11006.
37 J. P. Reid, B. J. Dennis-Smither, N. O. A. Kwamena, R. E. H. Miles, K. L. Hanford and C. J. Homer, *Phys. Chem. Chem. Phys.*, 2011, **13**, 15559–15572.
38 B. J. Dennis-Smither, K. L. Hanford, N. O. A. Kwamena, R. E. H. Miles and J. P. Reid, *J. Phys. Chem. A*, 2012, **116**, 6159–6168.
39 Y. You, *et al.*, *Proc. Natl. Acad. Sci. U. S. A.*, 2012, **109**, 13188–13193.
40 S. Langer, R. S. Pemberton and B. J. Finlayson-Pitts, *J. Phys. Chem. A*, 1997, **101**, 1277–1286.
41 F. Karagulian, C. W. Dilbeck and B. J. Finlayson-Pitts, *J. Phys. Chem. A*, 2009, **113**, 7205–7212.

42 C. C. Lai, S. Yang and B. J. Finlayson-Pitts, *Langmuir*, 1994, **10**, 4637–4644.
43 Y. Wadia, D. J. Tobias, R. Stafford and B. J. Finlayson-Pitts, *Langmuir*, 2000, **16**, 9321–9330.
44 M. L. E. TeVrucht and P. R. Griffiths, *Appl. Spectrosc.*, 1989, **43**, 1492–1494.
45 G. J. Kipouros and D. R. Sadoway, *J. Light Met.*, 2001, **1**, 111–117.
46 H. Shaka, W. H. Robertson and B. J. Finlayson-Pitts, *Phys. Chem. Chem. Phys.*, 2007, **9**, 1980–1990.
47 S. Kashani-Nejad, K. Ng and R. Harris, *Metall. Mater. Trans. B*, 2004, **35**, 405–406.
48 S. Twomey, *J. Appl. Phys.*, 1953, **24**, 1099–1102.
49 S. P. Sander, *et al.*, *Chemical Kinetics and Photochemical Data for Use in Atmospheric Studies, Evaluation No. 17*, JPL Publication 10-6, Jet Propulsion Laboratory, Pasadena, 2011.
50 G. Socrates, *Infrared and Raman Characteristic Group Frequencies*, John Wiley & Sons, New York, 2001.
51 J. L. R. Arrondo, F. M. Goni and J. M. Macarulla, *Biochim. Biophys. Acta*, 1984, **794**, 165–168.
52 P. T. T. Wong and H. H. Mantsch, *Chem. Phys. Lipids*, 1988, **46**, 213–224.
53 Y. Dubowski, J. Vieceli, D. J. Tobias, A. Gomez, A. Lin, S. Nizkorodov, T. McIntire and B. J. Finlayson-Pitts, *J. Phys. Chem. A*, 2004, **108**, 10473–10485.
54 T. M. McIntire, O. Ryder and B. J. Finlayson-Pitts, *J. Phys. Chem. C*, 2009, **113**, 11060–11065.
55 S. G. Moussa and B. J. Finlayson-Pitts, *Phys. Chem. Chem. Phys.*, 2010, **12**, 9419–9428.
56 S. G. Moussa, A. C. Stern, J. D. Raff, C. W. Dilbeck, D. J. Tobias and B. J. Finlayson-Pitts, *Phys. Chem. Chem. Phys.*, 2013, **15**, 448–458.
57 R. Criegee and H. Korber, *Chem. Ber.*, 1971, **104**, 1807–1811.
58 P. S. Bailey, *Ozonation in Organic Chemistry*, Academic Press, New York, 1978.
59 B. J. Finlayson-Pitts and J. N. Pitts Jr, *Chemistry of the Upper and Lower Atmosphere – Theory, Experiments, and Applications*, Academic Press, San Diego, 2000.
60 D. Johnson and G. Marston, *Chem. Soc. Rev.*, 2008, **37**, 699–716.
61 S. Gäb, E. Hellpointer, W. V. Turner and F. Korte, *Nature*, 1985, **316**, 535–536.
62 S. Hatakeyama and H. Akimoto, *Res. Chem. Intermed.*, 1994, **20**, 503–524.
63 W. A. Pryor, *Free Radical Biol. Med.*, 1994, **17**, 451–465.
64 O. Horie, P. Neeb, S. Limbach and G. K. Moortgat, *Geophys. Res. Lett.*, 1994, **21**, 1523–1526.
65 H. J. Tobias and P. J. Ziemann, *J. Phys. Chem. A*, 2001, **105**, 6129–6135.
66 O. Welz, J. D. Savee, D. L. Osborn, S. S. Vasu, C. J. Percival, D. E. Shallcross and C. A. Taatjes, *Science*, 2012, **335**, 204–207.
67 H. Kuhne and H. Gunthard, *J. Phys. Chem.*, 1976, **80**, 1238–1247.
68 L. Andrews and C. K. Kohlmiller, *J. Phys. Chem.*, 1982, **86**, 4548–4557.
69 M. Hawkins, C. K. Kohlmiller and L. Andrews, *J. Phys. Chem.*, 1982, **86**, 3154–3166.
70 C. C. Lai, B. J. Finlayson-Pitts and W. V. Willis, *Chem. Res. Toxicol.*, 1990, **3**, 517–523.
71 U. Samuni, Y. Haas, R. Fajgar and J. Pola, *J. Mol. Struct.*, 1998, **449**, 177–201.
72 R. Fajgar, J. Vitek, Y. Haas and J. Pola, *J. Chem. Soc., Perkin Trans.*, 1999, **2**, 239–248.
73 S. A. Epstein and N. M. Donahue, *J. Phys. Chem. A*, 2008, **112**, 13535–13541.
74 E. R. Thomas, G. J. Frost and Y. Rudich, *J. Geophys. Res.*, 2001, **106**, 3045–3056.
75 G. Y. Stokes, A. M. Buchbinder, J. M. Gibbs-Davis, K. A. Scheidt and F. M. Geiger, *J. Phys. Chem. A*, 2008, **112**, 11688–11698.
76 G. Y. Stokes, A. M. Buchbinder, J. M. Gibbs-Davis, K. A. Scheidt and F. M. Geiger, *Vib. Spectrosc.*, 2009, **50**, 86–98.
77 C. W. Harmon, S. A. Mang, J. Greaves and B. J. Finlayson-Pitts, *J. Chem. Educ.*, 2010, **87**, 186–189.
78 R. P. Schwarzenbach, P. M. Gschwend and D. M. Imoben, *Environmental Organic Chemistry*, Wiley, Hoboken, N.J., 2003.
79 V. F. McNeill, G. M. Wolfe and J. A. Thornton, *J. Phys. Chem. A*, 2007, **111**, 1073–1083.
80 O. Vesna, M. Sax, M. Kalberer, A. Gaschen and M. Ammann, *Atmos. Environ.*, 2009, **43**, 3662–3669.
81 J. Vieceli, O. L. Ma and D. J. Tobias, *J. Phys. Chem. A*, 2004, **108**, 5806–5814.
82 M. Hallquist, *et al.*, *Atmos. Chem. Phys.*, 2009, **9**, 5155–5236.
83 Y. Ma, T. Luciani, R. A. Porter, A. T. Russell, D. Johnson and G. Marston, *Phys. Chem. Chem. Phys.*, 2007, **9**, 5084–5087.
84 P. Neeb, F. Sauer, O. Horie and G. K. Moortgat, *Atmos. Environ.*, 1997, **31**, 1417–1423.
85 J. G. Calvert, R. Atkinson, J. A. Kerr, S. Madronich, G. K. Moortgat, T. J. Wallington and G. Yarwood, *The Mechanisms of Atmospheric Oxidation of the Alkenes*, Oxford University Press, Oxford, 2000.
86 W. A. Pryor and D. F. Church, *Free Radical Biol. Med.*, 1991, **11**, 41–46.
87 W. A. Pryor, B. Das and D. F. Church, *Chem. Res. Toxicol.*, 1991, **4**, 341–348.
88 J. Santrock, R. A. Gorski and J. F. O'Gara, *Chem. Res. Toxicol.*, 1992, **5**, 134–141.
89 F. Sauer, C. Schafer, P. Neeb, O. Horie and G. K. Moortgat, *Atmos. Environ.*, 1999, **33**, 229–241.
90 H. J. Tobias, K. S. Docherty, D. E. Beving and P. J. Ziemann, *Environ. Sci. Technol.*, 2000, **34**, 2116–2125.
91 B. Warscheid and T. Hoffmann, *Atmos. Environ.*, 2001, **35**, 2927–2940.
92 R. Tillmann, M. Hallquist, A. M. Jonsson, A. Kiendler-Scharr, H. Saathoff, Y. Iinuma and T. F. Mentel, *Atmos. Chem. Phys.*, 2010, **10**, 7057–7072.

93 H. I. Kim, H. Kim, Y. S. Shin, L. W. Beegle, W. A. Goddard, J. R. Heath, I. Kanik and J. L. Beauchamp, *J. Phys. Chem. B*, 2010, **114**, 9496–9503.
94 G. L. Squadrito, R. M. Uppu, R. Cueto and W. A. Pryor, *Lipids*, 1992, **27**, 955–958.
95 W. A. Pryor and M. Wu, *Chem. Res. Toxicol.*, 1992, **5**, 505–511.
96 K. Sabatini, J. P. Mattila, F. M. Megli and P. K. J. Kinnunen, *Biophys. J.*, 2006, **90**, 4488–4499.
97 M. Khabiri, M. Roeselová and L. Cwiklik, *Chem. Phys. Lett.*, 2012, **519–520**, 93–99.
98 J. Wong-Ekkabut, Z. T. Xu, W. Triampo, I. M. Tang, D. P. Tieleman and L. Monticelli, *Biophys. J.*, 2007, **93**, 4225–4236.
99 H. Khandelia and O. G. Mouritsen, *Biophys. J.*, 2009, **96**, 2734–2743.
100 L. Cwiklik and P. Jungwirth, *Chem. Phys. Lett.*, 2010, **486**, 99–103.
101 P. Jurkiewicz, A. Olzynska, L. Cwiklik, E. Conte, P. Jungwirth, F. M. Megli and M. Hof, *Biochim. Biophys. Acta Biomembr.*, 2012, **1818**, 2388–2402.
102 T. Koop, A. Kapilashrami, L. T. Molina and M. J. Molina, *J. Geophys. Res.*, 2000, **105**, 26393–26402.
103 I. N. Tang and H. R. Munkelwitz, *Atmos. Environ.*, 1993, **27**, 467–473.
104 I. N. Tang and H. R. Munkelwitz, *J. Appl. Meteorol.*, 1994, **33**, 791–796.
105 M. E. Wise, S. T. Martin, L. M. Russell and P. R. Buseck, *Aerosol Sci. Technol.*, 2008, **42**, 281–294.
106 I. N. Tang, A. C. Tridico and K. H. Fung, *J. Geophys. Res.*, 1997, **102**, 23,269–23,275.
107 M. E. Wise, T. A. Semeniuk, R. Bruintjes, S. T. Martin, L. M. Russell and P. R. Buseck, *J. Geophys. Res.*, 2007, **112**, DOI: 10.1029/2006jd007678.
108 J. Ofner, N. Balzer, J. Buxmann, H. Grothe, P. Schmitt-Kopplin, U. Platt and C. Zetzsch, *Atmos. Chem. Phys.*, 2012, **12**, 5787–5806.
109 R. von Glasow and P. J. Crutzen, in *Treatise on Geochemistry*, ed. H. D. Holland and K. Turekian, Elsevier Pergamon, Amsterdam, San Diego, 2007, vol. 4.02, pp. 1–67.

